Proceedings of the ASME 2015 Manufacturing Science and Engineering Conference
MSEC2015
June 8-12, 2015, Charlotte, NC, USA

MSEC2015-9395

HEAT TREATMENT RESPONSE OF STEEL FATIGUE SAMPLE DURING VACUUM CARBURIZATION AND HIGH PRESSURE GAS QUENCHING PROCESS

Zhichao (Charlie) Li, PhD
DANTE Solutions, Inc.
7261 Engle Road, Suite 105
Cleveland, Ohio, USA
Charlie.Li@Dante-Solutions.com

KEYWORDS
Vacuum carburization, High pressure gas quenching, Quench hardening, Residual stress, Distortion.

ABSTRACT
A hollow R.R. Moore rotation fatigue sample made of AISI 9310 is processed using vacuum carburization and high pressure gas quenching. The vacuum carburization schedule is designed to through carburize the thin wall section of the fatigue sample to 0.7% wt.% carbon, followed by 10 bar nitrogen quench. Some samples showed significant bow distortion after quench hardening, and further investigations indicated that the unbalanced wall thickness from machining is the main cause of the bow distortion. In this paper, DANTE, a commercial heat treatment software is used to study the cooling, phase transformation, and stress evolution during quenching. The effect of unbalance wall thickness on distortion is also investigated. Residual stress state in the quench hardened sample is critical to the fatigue performance during rotational bending fatigue tests. In this study, the unbalanced geometry has insignificant effect on the residual stresses after quench hardening. However, the unbalanced geometry will affect the applied stress significantly during a rotation fatigue test.

INTRODUCTION
Vacuum carburization has become more popular in steel heat treatment industry over the past decades. Comparing to the traditional gas carburization process, the vacuum carburization process reduces the total furnace time, and more flexibly controls the carbon profile in the case depth [1-2]. Two major gases are commonly used in vacuum carburization process: acetylene and propane. The acetylene has better penetration property over propane, which can provide more uniform carbon through small deep-hole geometries. The carbon content in steel affects its hardness and strength, and the carbon content significantly affects the phase transformation kinetics during quench hardening. Higher carbon content increases the incubation time and decreases the rate of diffusive phase transformations during cooling processes. Higher carbon content also decreases the martensitic phase transformation starting temperature (Ms). The effect of carbon content on phase transformations affects the internal stress evolution and shape change of the part during a quenching process. Because the vacuum carburization process has more flexible control on the carbon distribution profile in the case, it leaves more room for process optimization to improve the residual stress state and reduce distortion of carburized and quench hardened parts.

In a quench hardening process, the material volume changes with phase transformations, and the distortion is inevitable in quench hardened parts [3-6]. The heat treatment distortion is closely dependent on the part geometry. In general, an unbalanced part geometry contributes to distortion. In this study, some machined hollow R.R. Moore samples have an offset wall thickness as shown in Figure 1.

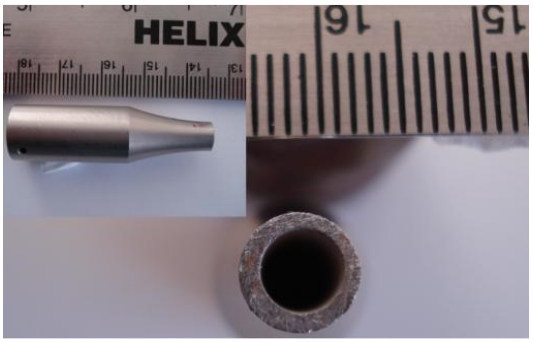

FIGURE 1 – PICTURE OF A ROTATION FATIGUE TEST SAMPLE SHOWING OFFSET WALL THICKNESS.

The offset geometry can lead to unbalanced carbon contents between the thinner and thicker wall sections from vacuum carburization process. During quenching, the thinner and thicker wall sections have different temperature, phase transformation and stress histories, which will lead to distortion in the hardened part. In this paper, the heat treatment process of the rotation fatigue sample is modeled using DANTE, a commercialized FEA based heat treatment software. The relation of the geometry effect on carburization, cooling rate, phase transformation and distortion is investigated.

FINITE ELEMENT MODELING

Sample Geometry and FEA Model

Half model is used in this study because both the perfect and offset samples have symmetric geometric feature. The CAD model and the brief sample dimensions are shown in Figure 2(a). The length of the coupon is 88.9 mm, its bore diameter is 4.775 mm, and it outer diameter at the mid-length position is 6.35 mm. The thinnest wall thickness is 0.7875 mm for the perfectly machined sample. It is observed that the hole has a maximum offset of 0.1 mm. In this study, two part geometries are modeled: 1) the first part has the perfect geometry, and 2) the second part has a hole offset of 0.1 mm. The thinner wall thickness is 0.6875 mm at the mid-length position, and its opposite side is the thicker wall with a wall thickness of 0.8875 mm.

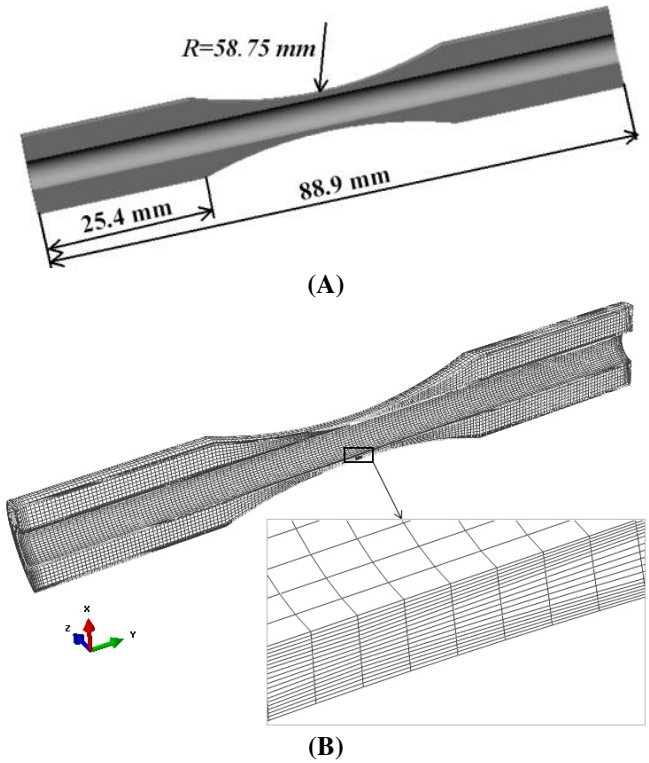

FIGURE 2 – (A) GEOMETRY OF THE ROTATION FATIGUE TEST COUPON, AND (B) FINITE ELEMENT MODEL.

The finite element model is shown in Figure 2(b). The model has 87096 nodes and 78660 linear hexagonal elements. Fine elements are used in the part surface to more accurately catch the gradients of carbon, temperature, phase transformation and stress during quench hardening process. The computational time for one heat treatment model is about 2 hours using a HP workstation with one 3.46 GHz quad-core processor.

Phase Transformation Kinetics

The fatigue sample is machined from extruded AISI 9310 steel bar. Phase transformation models are required to model the quench hardening processes [7-8]. The diffusive and martensitic transformation models in DANTE are described in equations (1) and (2) below.

$$\frac{d\Phi_d}{dt} = \nu_d(T)\Phi_d^{\alpha 1}(1-\Phi_d)^{\beta 1}\Phi_a \quad (1)$$

$$\frac{d\Phi_m}{dT} = \nu_m(1-\Phi_m)^{\alpha 2}(\Phi_m + \varphi\Phi_d)^{\beta 2}\Phi_a \quad (2)$$

where Φ_d and Φ_m are the volume fractions of individual diffusive phase and martensite transformed from austenite; Φ_a is the volume fraction of austenite; ν_d and ν_m are the mobilities of tranformation; ν_d is a function of temperature, and ν_m is a constant; $\alpha 1$ and $\beta 1$ are the constants of diffusive transformation; $\alpha 2$, $\beta 2$ and φ are constants of martensitic transformation. For each individual phase formation, one set of transformation kinetics parameters is required.

Figure 3(a) is a continuous cooling dilatometry strain curve generated from DANTE database representing martensitic transformation of AISI 9310. The horizontal axis in Figure 3(a) is the temperature, and the vertical axis is strain. The strain change due to martensitic transformation is clearly quantified.

When the dilatometry test sample cools to the Ms, its volume expands with the crystal strucure change from austenite's face centered cubic (FCC) lattice to martensite's body centered tetragonal (BCT) lattice. Martensite's BCT structure has a lower density than austenite's FCC structrue. The strain change during transformation is a combination of thermal strain, phase transformation volume change, and strain induced by stresses generated during the transformation. The latter strain is referred to as TRansformation Induced Plasticity or TRIP. The data obtained from this specific dilatometry test include coefficient of thermal expansion (CTE) for austensite and martensite, martensitic transformation starting and finishing temperature (Ms, Mf), transformation strain, and phase transformation kinetics (transformation rate) from austenite to martensite. These data are critical to the accuracy of modeling the internal stress and deformation caused by quenching.

Diffusive transformations are also characterized by dilatometry tests. A series of dilatometry tests with different cooling rates are required to fit a full set of diffusive and martensitic phase transformation kinetics parameters. Once the full set of phase transformation kinetics paratmeters are fit from dilatometry tests, isothermal transformation (TTT) and continuous cooling transformation (CCT) diagrams can be

generated for users to review. TTT/CCT diagrams are not directly used by DANTE phase transformation kinetics models, but they are useful because users can see the hardenability of the material graphically. Figure 3(b) is an isothermal transformation diagram (TTT) for 9310 steel created from the DANTE database.

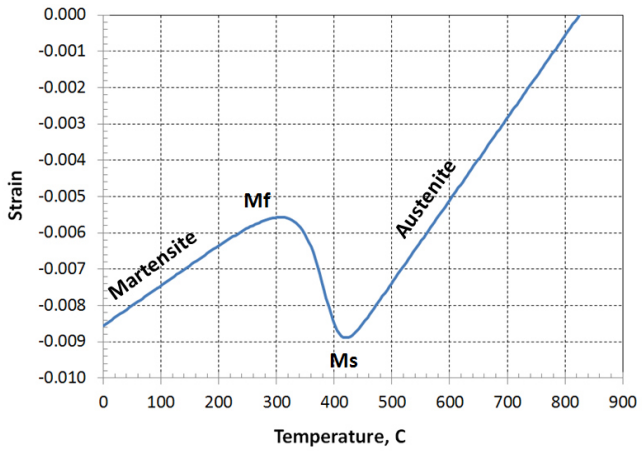

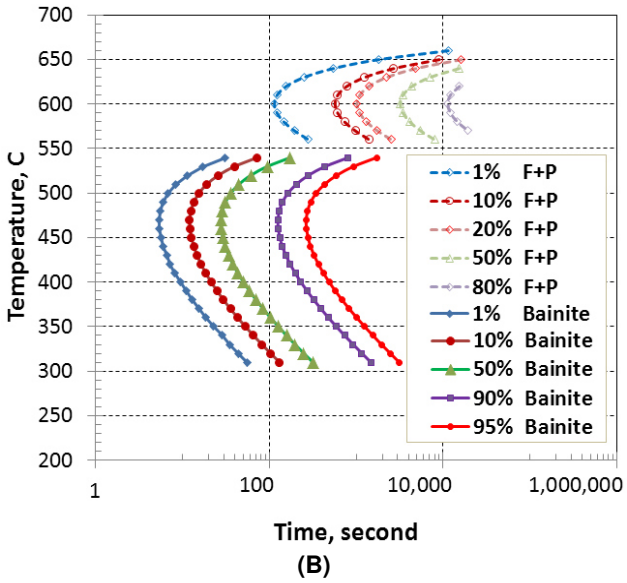

FIGURE 3 – (A) DILATOMETRY STRAIN CURVE DURING CONTINUOUS COOLING, AND (B) TTT DIAGRAMS OF AISI 9310 GENERATED FROM DANTE DATABASE.

VACUUM CARBURIZATION PROCESS MODELING

The material of the rotation fatigue test sample is AISI 9310 with 0.1 wt.% base carbon. During the rotation bending fatigue test, the material at the mid-length location is tested by applying cyclic loading with rotation of the sample. To test the material performance with higher carbon content of AISI 9310, vacuum carburization is used to increase the carbon content at the mid-length location to 0.7 wt.%. Different from conventional gas carburization process, multiple boost/diffuse (B/D) steps are used in vacuum carburization. During boost process, acetylene cracks on the part surface, and the equilibrium carbon is reached on the surface in a short time. A diffuse process is followed after the boost to allow carbon diffuses from surface inward, and the carbon content drops on the surface. The diffuse process is important to avoid large carbide formation on the surface, which will block the carbon diffusion rate. The B/D schedule used in this study is listed in Table 1. The schedule includes a total of eight (8) B/D steps. A long final diffuse is applied to allow the carbon uniformly to distribute through the thin wall at the mid-length location. The furnace temperature for the vacuum carburization is 900 °C. After carburization, the samples are quenched directly using 10 bar high pressure gas quench.

Table 1: Vacuum Carburization Boost/Diffuse Schedule.

Schedule	Boost Time (s)	Diffuse Time (s)
1	270	195
2	90	285
3	75	360
4	75	435
5	75	510
6	75	585
7	75	675
8	60	7200

Two sample geometries are modeled: 1) the perfect sample, and 2) the offset sample. Figure 4 shows the predicted carbon distribution contour of the perfect geometry. The sample has various wall thickness in the middle section, and the thinnest wall is at the mid-length location. The mid-length region of the sample is through carburized, and the carbon gradient exists in regions toward the axial ends, where the geometry has a pure ring feature.

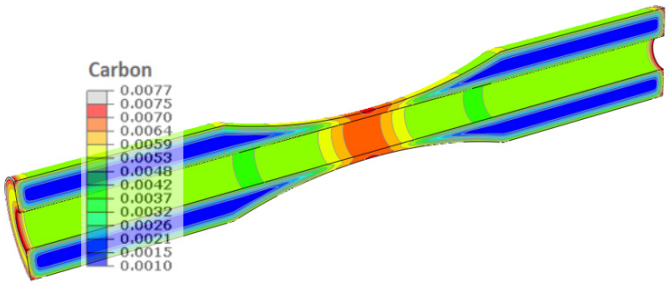

FIGURE 4 – CARBON DISTRIBUTION CONTOUR OF THE PERFECT SAMPLE.

Figure 5 shows the carbon distributions cross the mid-length wall after each B/D step. The horizontal axis is the depth from the outer surface. The X = 0 mm represents an outer surface point, and the X = 0.7875 mm represents an inner surface point. After the 7th B/D step, the carbon at the core of the wall is about 0.47 wt.%. With the final boost and long diffuse, the carbon level on the OD surface point is slightly higher than that of the ID surface point, which is purely due to the geometric effect. The

OD surface has a convex shape in the circumferential direction, and the ID surface has a concave shape. The surface to mass ratio of the OD surface is higher, which means more carbon diffuses into a unit mass on the OD surface than that to the ID surface. The average carbon level through the wall is about 0.7% as shown by the BD-8 curve in Figure 5.

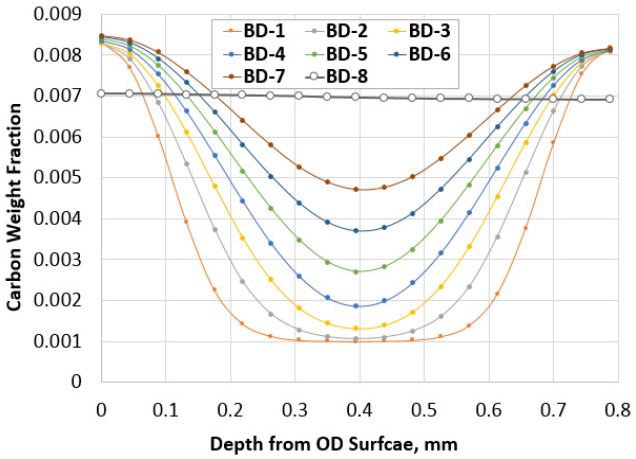

FIGURE 5 – CARBON DISTRIBUTIONS AFTER EACH BOOST/DIFFUSE STEP FOR THE ROTATION TEST COUPON WITH PERFECT GEOMETRY.

The offset sample assumes the hole has an offset of 0.1 mm. Therefore, the thickness of the thinner wall is 0.6875 mm, and the thickness of the thicker wall is 0.8875 mm. With the same vacuum carburization schedule listed in Table 1, the predicted carbon distribution contour is shown in Figure 6. The difference of the carbon contents between the thinner and the thicker wall is significant.

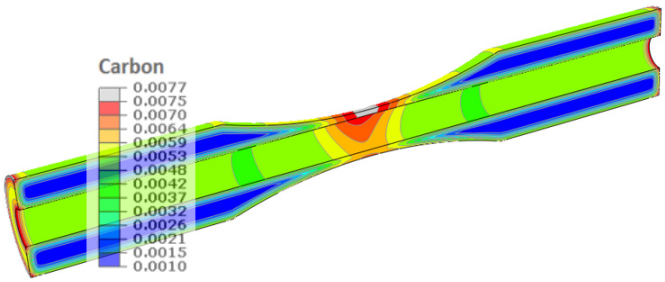

FIGURE 6 – CARBON DISTRIBUTION OF OFFSET ROTATION TEST COUPON.

Figures 7 and 8 show the predicted carbon distributions after each B/D step through the thinner and the thicker wall section respectively. The thinner wall has less mass than the thicker wall, and the carbon content after each B/D step at the core is higher in the thinner wall. After the final B/D step, the carbon distribution cross the wall is relatively uniform, and they are 0.65 wt.% through the thicker wall, and 0.78 wt.% through the thinner wall as shown in Figure 9, respectively.

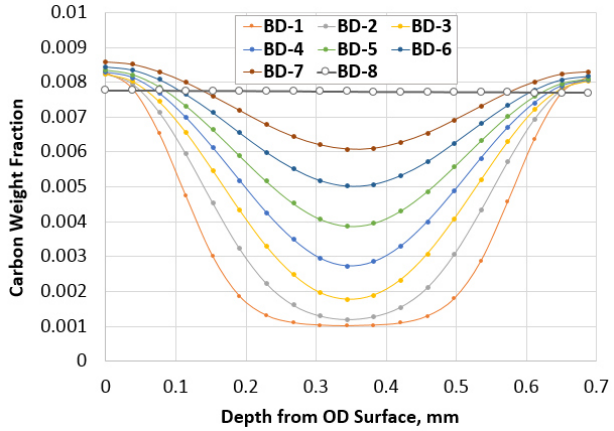

FIGURE 7 – CARBON DISTRIBUTIONS AFTER EACH BOOST/DIFFUSE STEP FOR THE ROTATION TEST COUPON WITH OFFSET WALL, THINNER WALL.

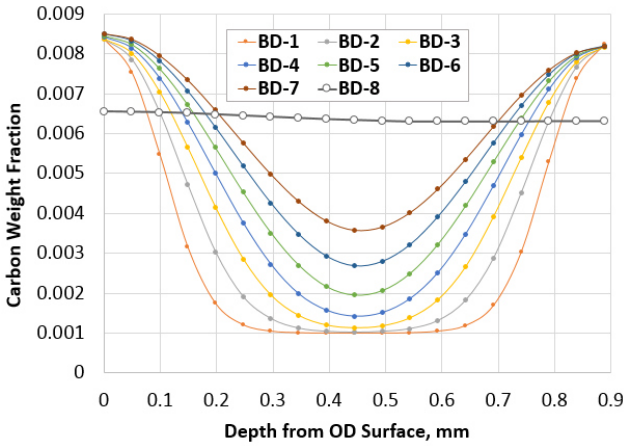

FIGURE 8 – CARBON DISTRIBUTIONS AFTER EACH BOOST/DIFFUSE STEP FOR THE ROTATION TEST COUPON WITH OFFSET WALL, THICKER WALL.

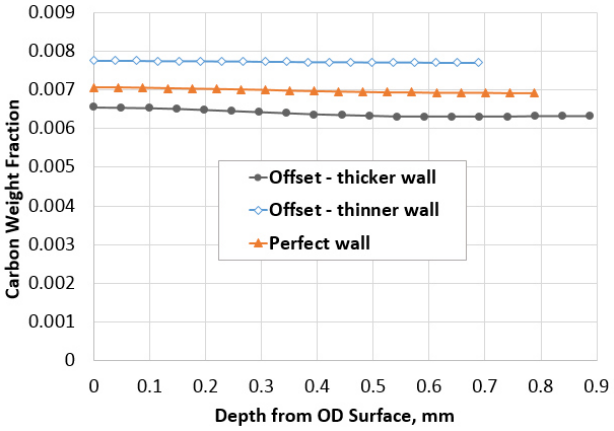

FIGURE 9 – COMPARISON OF FINAL CARBON DISTRIBUTIONS.

QUENCH HARDENING PROCESS MODELING

After carburization, the samples are quench hardened using 10bar high pressure gas quenching process. A constant heat transfer coefficient of 600 W/(m^{2}K) is applied to the outer surface of the sample to simulate the hardening process. It is assumed that the inner surface has a severe stagnant gas flow, and the heat transfer coefficient applied is 200 W/(m^{2}K). This thermal boundary condition is applied to both the perfect and offset samples. Using the offset sample as an example, the temperature and martensite distributions at 17.7 s in quenching are shown in Figure 10. The predicted temperature at the mid-length region is lower because it has a thinner wall relative to other locations. The martensite transformation is a function of temperature and carbon content. With higher carbon, the Ms decreases, and the martensite transformation starts under the carburized surface, as shown in Figure 10(a).

The wall thickness affects the temperature of the wall. Under the same thermal boundary conditions, the thinner wall has faster cooling rate than its opposite side (the thicker wall). For this offset fatigue test sample, the temperature distribution is nonuniform in the circumferential direction of the mid-length wall section, as shown in Figure 10(b).

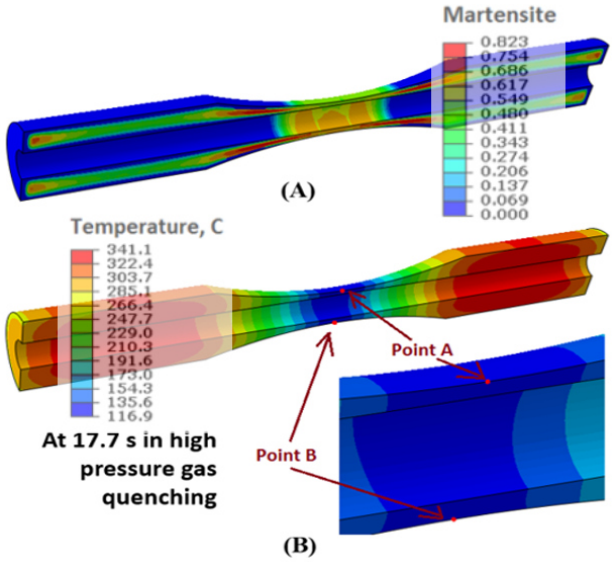

FIGURE 10 – (A) MARTENSITE, AND (B) TEMPERATUIRE DISTRIBUTION AT 17.7 S DURING GAS QUENCHING OF OFFSET SAMPLE.

To more clearly describe the effect of the offset geometry on the sample responses during quenching, two points are selected to plot histories of the temperature and phase transformation: 1) point A represents the outer surface of the thinner wall, and 2) point B represents the outer surface of the thicker wall, as shown in Figure 10(b). The horizontal axis in Figure 11 is the quenching time, with X = 0.0 s representing the stating time of the quenching. The major vertical axis is the temperature, and the second vertical axis is the volume fractions of phases. Point A cools faster than point B, and the maximum temperature difference between the two points is about 30 °C during quenching. AISI 9310 has a relatively high hardenability, especially in the thin wall region of the sample with higher carbon content. The only phase obtained under this gas quenching process is martensite as shown in Figure 11. The maximum phase (austenite or martensite) volume fraction difference during quenching is 15.9% between points A and B.

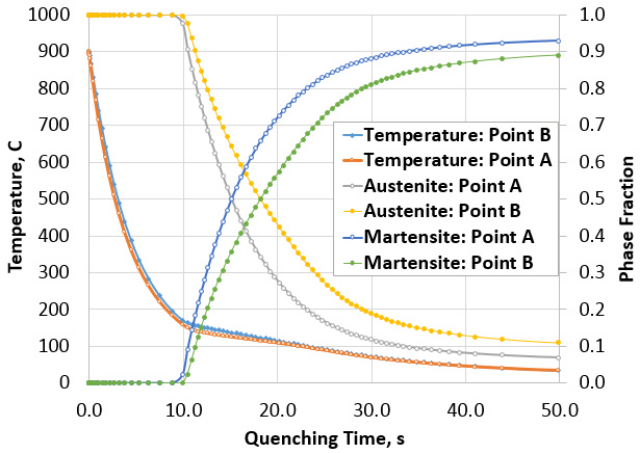

FIGURE 11 – DIFFERENCE OF TEMPERATURE AND PHASE TRANSFORMATIONS AT THE SURFACE POINTS A AND B OF THE OFFSET SAMPLE DURING QUENCHING.

Both temperature gradient and phase transformations contribute to the stress evolution of the sample during quenching process. In general, a carburized steel part ends up with compressive residual stress in the carburized case after quench hardening due to the delayed martensite transformation on the surface. As shown in Figure 12, the surface residual stress in the axial direction is in compressive in the region away from the mid-length region due to the carbon gradient through the wall. The thin wall section of the sample is through carburized with a relatively uniform carbon through the wall, as shown in Figure 9, and the axial residual stress distribution in this region is relatively uniform. The residual stress difference between the perfect sample and the offset sample is insignificant.

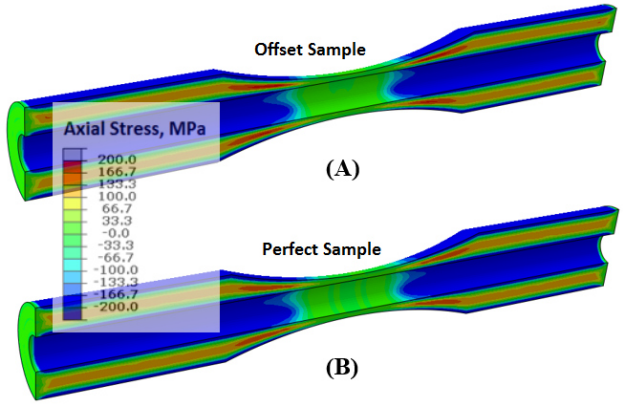

FIGURE 12 – RESIDUAL STRESS DISTRIBUTIONS: (A) OFFSET SAMPLE, AND (B) PERFECT SAMPLE.

The predicted distortion (axial bow) for both the perfect sample and the offset sample are shown in Figure 13. The black mesh represents the original shape, and the displacement are magnified by 50 times in Figures 13 (a) and (b). It clearly shows the bow distortion in the offset sample, and the perfect sample has no bow distortion. The sample geometry and the hardening distortion have significant effect on the uniformity of the applied stress in the test region (mid-length) during rotation bending fatigue test.

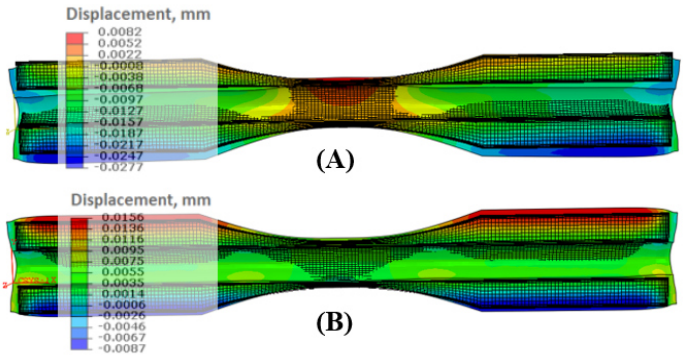

FIGURE 13 – DISTORTION COMPARISON AFTER QUENCH HARDENING. (A) OFFSET SAMPLE, AND (B) PERFECT SAMPLE (DISPLACEMENT 50X).

SUMMARY

Vacuum carburization and high pressure gas quenching process of a rotation bending fatigue sample are modeled. The effect of imperfect sample geometry from machining process on the part responses during hardening is studied by investigating its effect on cooling, phase transformation and stress evolution. It is found that the geometric effect on the residual stress distribution is insignificant. However, the effect of offset geometry on the distortion is significant. Both the offset wall thickness and the distortion will affect the applied stress in the sample during rotation bending fatigue test.

REFERENCES

[1] Hoffmann, F.T., Lubben, T., Mayr, P., "Innovations in Quenching Systems and Equipment: Current Status and Future Development", Heat Treat. Metals 26 (3) (1999), pp. 63–67.

[2] Lubben, T., Hoffmann, F.T., Mayr, P., Laumen, C., "The Uniformity of Cooling in High-Pressure Gas Quenching", Heat Treat. Metals, 27 (3) (2000), pp. 57–61.

[3] Ferguson, B., and Dowling, W., "Predictive Model and Methodology for Heat Treatment Distortion", NCMS Report #0383RE97, 1997.

[4] Bammann, D., et al., "Development of a Carburizing and Quenching Simulation Tool: A Material Model for Carburizing Steels Undergoing Phase Transformations", Proceedings of the 2nd International Conference on Quenching and the Control of Distortion, November (1996), pp. 367-375.

[5] Carlone, P., Palazzo, G. S., "Development and Validation of a Thermo-Mechanical Finite Element Model of the Steel Quenching Process Including Solid-Solid Phase Changes", Int. Appl. Mech. 46 (2011) 8, pp. 955-971.

[6] Warke, V., Sisson, R., and Makhlouf, M., "FEA Model for Predicting the Response of Powder Metallurgy Steel Components to Heat Treatment", Mater. Sci. Eng., A, 2009, 518(1–2), pp. 7–15.

[7] Li, Z., Ferguson, B., and Freborg, A., "Data Needs for Modeling Heat Treatment of Steel Parts", Proceedings of Materials Science & Technology Conference, 2004, pp. 219-226.

[8] Lusk, M., Wang, W., Sun, X.G., and Lee, Y.K., "On the Role of Kinematics in Constructing Predictive Models of Austenite Decomposition", Proceedings of TMS, Warrendale, PA, 2003, pp. 311–331.